

# Observation of an Emergent Coherent State in Iron-Based Superconductor $\text{KFe}_2\text{As}_2$

Run Yang,<sup>1,2,3</sup> Zhiping Yin,<sup>4,\*</sup> Yilin Wang,<sup>2</sup> Yaomin Dai,<sup>2</sup> Hu Miao,<sup>2</sup> Bing Xu,<sup>1</sup> Xianggang Qiu,<sup>1,3,5,†</sup> and Christopher C. Homes<sup>2,‡</sup>

<sup>1</sup>*Beijing National Laboratory for Condensed Matter Physics, Institute of Physics, Chinese Academy of Sciences, Beijing 100190, China*

<sup>2</sup>*Condensed Matter Physics and Materials Science Division, Brookhaven National Laboratory, Upton, New York 11973, USA*

<sup>3</sup>*School of Physical Sciences, University of Chinese Academy of Sciences, Beijing 100049, China*

<sup>4</sup>*Center for Advanced Quantum Studies and Department of Physics, Beijing Normal University, Beijing 100875, China*

<sup>5</sup>*Collaborative Innovation Center of Quantum Matter, Beijing 100084, China*  
(Dated: November 20, 2021)

The optical properties of  $\text{KFe}_2\text{As}_2$  have been measured for light polarized in the  $a$ - $b$  planes over a wide temperature and frequency range. Below  $T^* \simeq 155$  K, where this material undergoes an incoherent-coherent crossover, we observed a new coherent response emerging in the optical conductivity. A spectral weight analysis suggests that this new feature arises out of high-energy bound states. Below about  $T_{\text{FL}} \simeq 75$  K the scattering rate for this new feature is quadratic in temperature, indicating a Fermi-liquid response. Theory calculations suggest this crossover is dominated by the  $d_{xy}$  orbital. Our results advocate for Kondo-type screening as the mechanism for the orbital-selective incoherent-coherent crossover in hole-overdoped  $\text{KFe}_2\text{As}_2$ .

PACS numbers: 72.15.-v, 74.70.-b, 78.30.-j

Investigating the role of electronic correlations in systems with large orbital degrees of freedom remains a key challenge in understanding the multi-orbital physics in iron-based superconductors (FeSCs) [1–7]. Previous investigations found that, due to Hund’s rule coupling, the electron correlations strongly depend on the band filling and are responsible for the electron-hole asymmetry in FeSCs [8, 9]. Electron doping weakens the correlations and finally results in Fermi-liquid (FL) behavior [10], while the hole doping makes the system more correlated [11], due to strong Hund’s rule coupling and closer proximity to half filling [9].  $\text{KFe}_2\text{As}_2$ , as an extremely hole-doped FeSC, shows strong electronic correlations and bad-metal behavior at high temperature. However, upon cooling, the electrons start to form coherent quasiparticles around  $T^* \sim 155$  K, and shows FL behavior below  $T_{\text{FL}} \simeq 75$  K [12–14]; this has prompted an extensive debate between the orbital-selective Mottness [6, 8, 15] and Hund’s rule coupling induced Kondo-type screening as the mechanism for the incoherent-coherent crossover [16–19].

In this Letter we examine the temperature dependence of the optical conductivity of  $\text{KFe}_2\text{As}_2$  to study the incoherent-coherent crossover. As the temperature is lowered across  $T^*$ , we observe that spectral weight is transferred from high ( $\simeq 2000 - 3000 \text{ cm}^{-1}$ ) to low ( $\lesssim 1000 \text{ cm}^{-1}$ ) energy region into a new emergent Drude peak, which displays a FL behavior below  $\simeq 75$  K. To further investigate this behavior we performed dynam-

ical mean field theory (DMFT) calculations that suggest that the incoherent-coherent crossover is governed by the  $d_{xy}$  orbital. The FL behavior indicates the Kondo-type screening of local spin moments, which is consistent with susceptibility [13] and transport measurements [20] and in agreement with the theoretical prediction [19, 21]. However, the absence of a Mott gap in the high-temperature optical spectra rules out the possibility of orbital-selective Mottness. Thus, we propose a Kondo-type screening as the mechanism responsible for the orbital-selective incoherent-coherent crossover in  $\text{KFe}_2\text{As}_2$ , which is close to half filling. This result introduces constraints for further theoretical investigations to understand the orbital physics as well as the pairing mechanism in FeSCs.

High-quality single crystals of  $\text{KFe}_2\text{As}_2$  with good cleavage planes (001) were synthesized using self-flux method [22]. The reflectance from freshly-cleaved surfaces has been measured over a wide temperature ( $\sim 4$  to 300 K) and frequency range ( $\sim 2 \text{ meV}$  to about 5 eV) at a near-normal angle of incidence for light polarized in the  $ab$ -planes using an *in situ* evaporation technique [23]. The optical conductivity has been determined from a Kramers-Kronig analysis of the reflectivity (the reflectivity and the details of the Kramers-Kronig analysis may be found in the Supplemental Information).

The temperature dependence of the optical conductivity  $\sigma_1(\omega)$  is shown in Fig. 1 in the infrared region. The free carrier response is typically a Lorentzian centered at zero frequency where the width at half maximum is the scattering rate. At high temperature, the conductivity is low and resembles a bad metal; the nearly flat frequency response indicates a large scattering rate, signaling an almost incoherent response. As the tempera-

\* yinzhiping@bnu.edu.cn

† xgqiu@iphy.ac.cn

‡ homes@bnl.gov

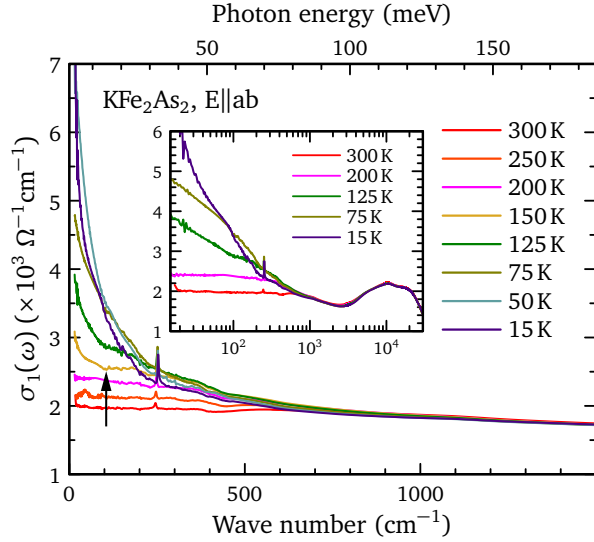


Figure 1. The temperature dependence of the real part of the optical conductivity of  $\text{KFe}_2\text{As}_2$  above and below the incoherent-coherent crossover  $T^*$ . Inset: The optical conductivity at several temperatures over a broad frequency range.

ture is reduced, the low-frequency conductivity increases gradually until 150 K, at which point a new Drude-like peak appears superimposed on the broad response, resulting in a kink in the low-energy conductivity (denoted by the arrow in Fig. 1, as well as the sudden change in slope in the inset). This new peak increases dramatically in strength and narrows quickly with decreasing temperature, reflecting its small scattering rate and coherent character [24].

Because of the multi-band nature of FeSCs there is typically more than one type of free carrier present. Consequently, to analyze the optical conductivity we employ a Drude-Lorentz model with multiple Drude components,

$$\sigma_1(\omega) = \frac{2\pi}{Z_0} \left[ \sum_j \frac{\omega_{p,j}^2 \tau_j}{(1 + \omega^2 \tau_j^2)} + \sum_k \frac{\gamma_k \omega^2 \Omega_k^2}{(\omega_k^2 - \omega^2)^2 + \gamma_k^2 \omega^2} \right], \quad (1)$$

where  $Z_0 \simeq 377 \Omega$  is the impedance of free space. The first term describes a sum of free-carrier Drude responses with plasma frequencies  $\omega_{p,j}^2 = 4\pi n_j e^2 / m_j^*$  ( $n_j$  represents the carrier concentration and  $m_j^*$  the effective mass), and scattering rates  $1/\tau_j$ . The second term is a sum of Lorentz oscillators with position  $\omega_k$ , width  $\gamma_k$ , and oscillator strength  $\Omega_k$ . At high temperature ( $T > 150$  K), the optical conductivity is described quite well by two Drude components and two Lorentz terms [Fig. S2(a) of the Supplementary Material]: a narrow Drude (D1) with a  $T$ -dependent scattering rate, a broad Drude (D2), which is almost  $T$  independent, indicating two groups of carriers [25, 26]. The narrow Drude reflects the coherent response and the broad Drude corresponds to the incoherent background. Below 150 K, the newly formed peak and corresponding kink in  $\sigma_1(\omega)$  makes it difficult

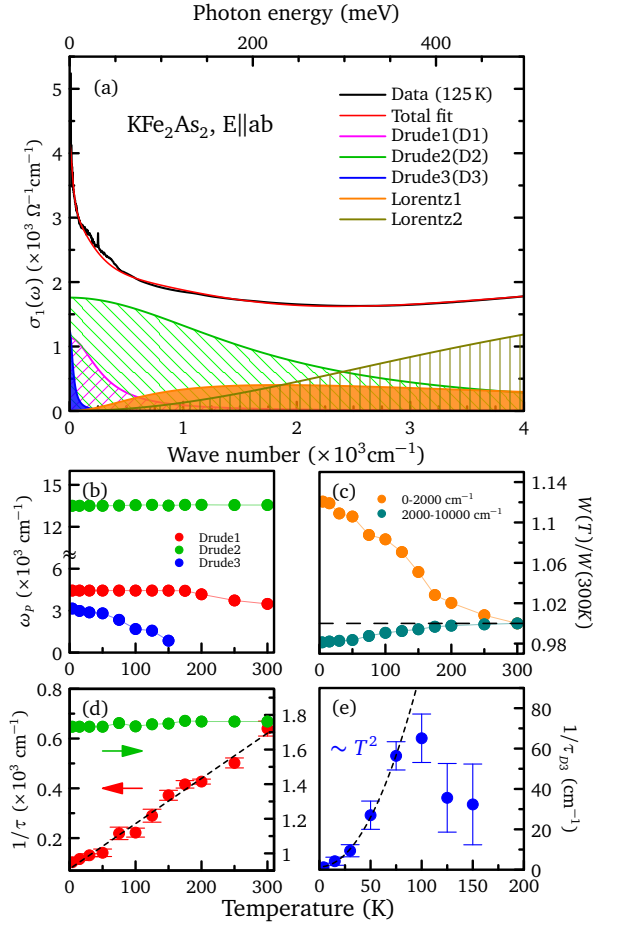


Figure 2. (a) Fit of the Drude-Lorentz model to the  $\sigma_1(\omega)$  of  $\text{KFe}_2\text{As}_2$  at 125 K, decomposed into individual Drude and Lorentz terms. (b) The plasma frequency  $\omega_p$  for the three Drude components. (c) Temperature dependence of the spectral weight,  $W(\omega_1, \omega_2, T)$ , for various lower and upper cutoff frequencies. (d) Scattering rates for the narrow Drude (D1) (red), broad Drude (D2) (green) components are extracted from the fits. The dashed line is the linear fit to  $1/\tau_{D1}$ . (e) The scattering rate of the emergent Drude component. The dashed line is the quadratic fit to  $1/\tau_{D3}$  below 75 K.

to fit the low-energy response with only two Drude components, so a third Drude component (D3) has been introduced. The existence of a new Drude component can also be realized by fitting the reflectivity and the imaginary part of the optical conductivity [Table I and Figs. S2 and S3 in the Supplementary Material].

Below  $T^*$  the data is reproduced quite well with three Drude and two Lorentz components, as illustrated by the fit to the data at 125 K in Fig. 2(a). The temperature dependence of the Drude components are summarized in Figs. 2(b-e). As the temperature is reduced, the values for  $\omega_p$  for the narrow and broad Drude terms, D1 and D2, respectively, remain essentially constant. Below  $T^*$  the plasma frequency for newly developed Drude component (D3) increases steadily and  $\omega_{p,D3}^2(T)$  follows a mean-field temperature dependence [Fig. S4(a) in the

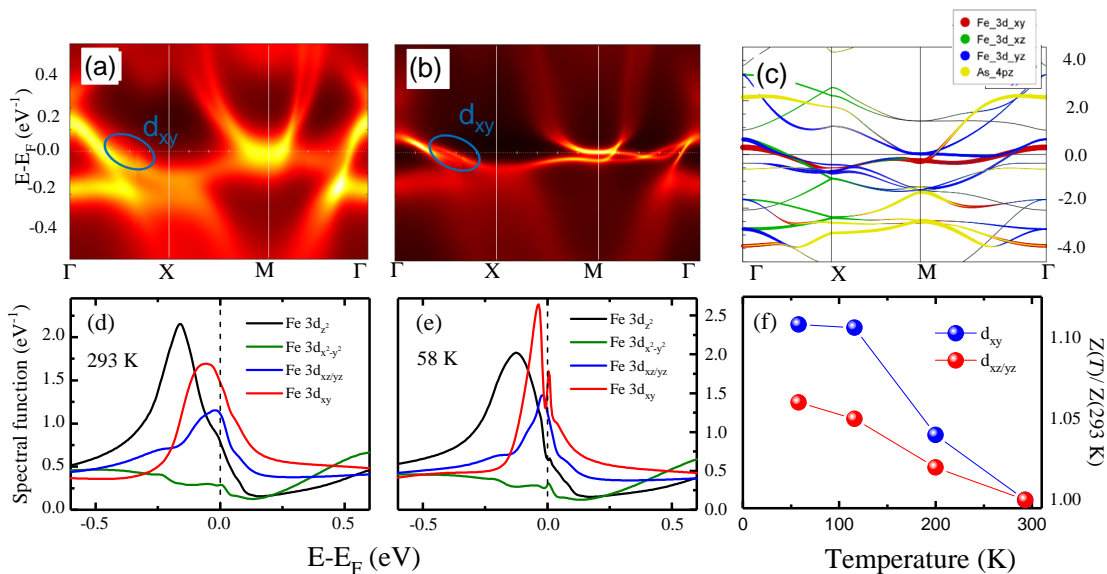


Figure 3. Electronic structure of  $KFe_2As_2$  above and below the incoherent-coherent crossover. (a) DFT+DMFT band structure for  $KFe_2As_2$  at 293 K and (b) 58 K; the blue ellipses denote the band of primarily  $d_{xy}$  character. (c) DFT band structure. (d) The Fe- $d$  orbital character for the density of states of  $KFe_2As_2$  at 293 K and (e) 58 K. (f) The temperature-dependent quasiparticle spectral weight  $Z$  calculate by integrating the spectral function near  $E_F$ .

Supplementary Material]. Figures 2(d) and 2(e) show the temperature dependence of the scattering rates;  $1/\tau_{D2}$  is almost temperature independent, while  $1/\tau_{D1} \propto T$ . Below  $T^*$ ,  $1/\tau_{D3}$  initially increases with temperature, but for  $T < T_{FL}$  FL behavior is observed,  $1/\tau_{D3} \propto T^2$ .

In order to understand the origin of the new peak (D3), we calculate the spectral weight of  $\sigma_1(\omega)$ ,

$$W(\omega_1, \omega_2, T) = \int_{\omega_1}^{\omega_2} \sigma_1(\omega, T) d\omega, \quad (2)$$

over different frequency intervals and normalize the result to the room-temperature value. In Fig. 2(c), we notice that, upon cooling, especially below 150 K, the spectral weight between  $\sim 0 - 2000\text{ cm}^{-1}$  is greatly enhanced, while the spectral weight in the high-energy range ( $2000 - 10000\text{ cm}^{-1}$ ) is suppressed. Since  $\omega_{p,D1}$  and  $\omega_{p,D2}$  are temperature-independent below 150 K, and the overall spectral weight up to  $10000\text{ cm}^{-1}$  remains constant [Fig. S3(a)] (the optical conductivity above  $10000\text{ cm}^{-1}$  does not vary with temperature), we propose that the new Drude component grows out of a high-energy bound state, indicating that some incoherent bands start to form coherent quasiparticles with an underlying Fermi surface, which is the typical signature for the incoherent-coherent crossover [19, 27]. Previous ARPES measurements [18, 28] observed a slight decrease of the spectral weight of a band near the Fermi level with increasing temperature. Here, we offer clear evidence of spectral weight transfer during this process in a system that is close to half filling.

Because D3's intensity is significantly enhanced and becomes very sharp at low temperatures, it dominates

the DC conductivity below 75 K [Fig. S2(b) in the Supplementary Material]; its  $T^2$ -dependent scattering rate, indicating FL behavior [29], is in agreement with recent transport measurements [20]. The ultra-low scattering rate for D3 reflects high quality of these samples (RRR  $\sim 512$ ); however, the presence of disorder might explain the absence of FL behavior observed in another study [30]. Comparing with D3, even though D1's contribution to the DC conductivity is very small, the existence of two different kinds of narrow Drude components points to strong orbital differentiation in FeSCs [9, 13].

To better understand the origin of the emergent Drude component, calculations for  $KFe_2As_2$  were performed using density functional theory (DFT), and extended using dynamical mean field theory (DMFT) (the details of which are described in the Supplemental Material); DFT+DMFT has been shown to accurately reproduce the electronic behavior of strongly correlated materials where DFT alone typically fails [2, 31, 32]. The results are summarized in Fig. 3. Consistent with ARPES measurements, only hole-like Fermi surfaces are present in  $KFe_2As_2$  [33, 34]. From the temperature-dependent band structure, we notice that at high temperature [293 K, Fig. 3(a)], the band with  $d_{xy}$  orbital character is much fainter than those dominated by the  $d_{xz/yz}$  orbitals. However, at low temperature [58 K, Fig. 3(b)] the  $d_{xy}$  character increases dramatically. These changes are reflected in the temperature dependence of the density-of-states (DOS) for different orbital characters [Fig. 3(d) at 293 K, and Fig. 3(e) at 58 K], where the  $d_{xy}$  DOS sharpens at low temperature and dominates the low-energy DOS, signalling an incoherent-coherent crossover. This suggests that the emergent coherent peak in the optical

conductivity below 150 K is most likely dominated by the  $d_{xy}$  orbital.

In most iron-based superconductors, the state near  $E_F$  arises mainly from the  $t_{2g}$  orbitals; correlation effects will give rise to charge transfer from the  $d_{xy}$  to  $d_{xz/yz}$  orbitals [35, 36]. Comparing the DFT+DMFT band structure in Fig. 3(b) with that of DFT in 3(c) [also see Fig. S5(b) in the Supplemental Material], the presence of electronic correlations leads to an increase in the contribution of the  $d_{xy}$  band to the Fermi surface, while the  $d_{xz/yz}$  contribution decreases in order to maintain the Luttinger count. In this hole-overdoped system ( $5.5e/Fe$ ), charge transfer pushes the  $d_{xy}$  orbital much closer to half filling [8], and Hund's rule coupling results in a strong renormalization of this orbital [8, 9], with the renormalization factor  $1/Z \propto U/t$ , where  $t$  is the hybridization magnitude and  $Z$  is the quasiparticle spectral weight. Thus, at high temperature the  $d_{xy}$  orbital is more incoherent (localized) and contributes to the local moment, resulting in a Curie-Weiss susceptibility [13]. At low temperature, the quasiparticle spectral weight (proportional to the hybridization of  $d_{xy}$  orbital between nearest-neighbor atoms), is enhanced continuously [37] [Fig. 3(f)]. Below 150 K, this orbital begins to delocalize and form coherent quasiparticles, which is consistent with the spectral transfer from the high to low-energy region [Fig. 2(c)] and the formation of a new coherent peak in our optical conductivity. Below 75 K, FL behavior ( $1/\tau_{D3} \propto T^2$ ) is observed. This result, combined with the Pauli-like susceptibility [13], indicates Kondo-type screening, during which the local moments are totally screened by the conduction electrons, resulting in a saturated spin susceptibility and diminished scattering from local spins [19].

The absence of this behavior in a simple DFT calculation indicates that this incoherent-coherent crossover is the result of electronic correlations driven by Hund's rule coupling [14, 16] (Fig. S5 in the Supplementary Ma-

terial). While the spectral weight in the optical conductivity is transferred from low to high-energy region upon warming, the absence of a gap-like structure in the optical conductivity and the residual DOS of the  $d_{xy}$  orbital near the Fermi level at 293 K are inconsistent with the description of an orbital-selective Mott transition [38]; instead, our observation suggests an orbital-selective incoherent-coherent crossover in a Hund's metal [19, 39, 40].

In summary, we have observed an emergent Drude peak in the optical conductivity of  $KFe_2As_2$  associated with the incoherent-coherent crossover below  $T^* \simeq 155$  K, and determined that it originates from a high-energy bound state. Below 75 K, this response sharpens quickly and shows FL behavior, which may come from Kondo-type screening by the delocalized electrons. Based on DFT+DMFT calculations, we find that this new peak is dominated by the  $d_{xy}$  orbital, reflecting an orbital-selective incoherent-coherent crossover. We propose that in  $KFe_2As_2$ , which is close to half filling, the incoherent-coherent crossover is related to Hund's rule driven Kondo-type screening, rather than orbital-selective Mottness.

#### ACKNOWLEDGMENTS

We thank I. Zaliznyak, A. Wang and W. Yin for useful discussions. Work at Chinese Academy of Science was supported by NSFC (Project No. 11374345 and No. 91421304) and MOST (Project No. 2015CB921303 and No. 2015CB921102). Work at Beijing Normal University was supported by the National Natural Science Foundation of China (Grant No. 11674030) and the National Key Research and Development Program of China (contract No. 2016YFA0302300). Work at Brookhaven National Laboratory was supported by the Office of Science, U.S. Department of Energy under Contract No. DE-SC0012704.

- 
- [1] P. Richard, T. Sato, K. Nakayama, S. Souma, T. Takahashi, Y.-M. Xu, G. F. Chen, J. L. Luo, N. L. Wang, and H. Ding, *Phys. Rev. Lett.* **102**, 047003 (2009).
  - [2] Z. P. Yin, K. Haule, and G. Kotliar, *Nature Mater.* **10**, 932 (2011).
  - [3] M. M. Qazilbash, J. J. Hamlin, R. E. Baumbach, L. Zhang, D. J. Singh, M. B. Maple, and D. N. Basov, *Nature Phys.* **5**, 647 (2009).
  - [4] A. Georges, L. de' Medici, and J. Mravlje, *Ann. Rev. Conden. Mat. Phys.* **4**, 137 (2013).
  - [5] R. Yu and Q. Si, *Phys. Rev. B* **84**, 235115 (2011).
  - [6] D. H. Lu, M. Yi, S.-K. Mo, A. S. Erickson, J. Analytis, J.-H. Chu, D. J. Singh, Z. Hussain, T. H. Geballe, I. R. Fisher, and Z.-X. Shen, *Nature* **455**, 81 (2008).
  - [7] X. Chen, P. Dai, D. Feng, T. Xiang, and F.-C. Zhang, *Nat. Sci. Rev.* **1**, 371 (2014).
  - [8] L. de Medici, G. Giovannetti, and M. Capone, *Phys. Rev. Lett.* **112**, 177001 (2014).
  - [9] L. de Medici, J. Mravlje, and A. Georges, *Phys. Rev. Lett.* **107**, 256401 (2011).
  - [10] F. L. Ning, K. Ahilan, T. Imai, A. S. Sefat, M. A. McGuire, B. C. Sales, D. Mandrus, P. Cheng, B. Shen, and H.-H. Wen, *Phys. Rev. Lett.* **104**, 037001 (2010).
  - [11] F. Hardy, A. E. Böhmer, L. de' Medici, M. Capone, G. Giovannetti, R. Eder, L. Wang, M. He, T. Wolf, P. Schweiss, R. Heid, A. Herbig, P. Adelman, R. A. Fisher, and C. Meingast, *Phys. Rev. B* **94**, 205113 (2016).
  - [12] F. Eilers, K. Grube, D. A. Zocco, T. Wolf, M. Merz, P. Schweiss, R. Heid, R. Eder, R. Yu, J.-X. Zhu, Q. Si, T. Shibauchi, and H. v. Löhneysen, *Phys. Rev. Lett.* **116**, 237003 (2016).
  - [13] F. Hardy, A. E. Böhmer, D. Aoki, P. Burger, T. Wolf, P. Schweiss, R. Heid, P. Adelman, Y. X. Yao, G. Kotliar, J. Schmalian, and C. Meingast, *Phys. Rev. Lett.* **111**, 027002 (2013).

- [14] K. Haule and G. Kotliar, *New J. Phys.* **11**, 025021 (2009).
- [15] Y. Liu, D.-Y. Liu, J.-L. Wang, J. Sun, Y. Song, and L.-J. Zou, *Phys. Rev. B* **92**, 155146 (2015).
- [16] L. Fanfarillo and E. Bascones, *Phys. Rev. B* **92**, 075136 (2015).
- [17] S. Backes, H. O. Jeschke, and R. Valentí, *Phys. Rev. B* **92**, 195128 (2015).
- [18] H. Miao, Z. P. Yin, S. F. Wu, J. M. Li, J. Ma, B.-Q. Lv, X. P. Wang, T. Qian, P. Richard, L.-Y. Xing, X.-C. Wang, C. Q. Jin, K. Haule, G. Kotliar, and H. Ding, *Phys. Rev. B* **94**, 201109 (2016).
- [19] K. M. Stadler, Z. P. Yin, J. von Delft, G. Kotliar, and A. Weichselbaum, *Phys. Rev. Lett.* **115**, 136401 (2015).
- [20] Z. J. Xiang, N. Z. Wang, A. F. Wang, D. Zhao, Z. L. Sun, X. G. Luo, T. Wu, and X. H. Chen, *J. Phys.: Condens. Matter* **28**, 425702 (2016).
- [21] C. Aron and G. Kotliar, *Phys. Rev. B* **91**, 041110 (2015).
- [22] J. S. Kim, E. G. Kim, G. R. Stewart, X. H. Chen, and X. F. Wang, *Phys. Rev. B* **83**, 172502 (2011).
- [23] C. C. Homes, M. Reedyk, D. A. Crandles, and T. Timusk, *Appl. Opt.* **32**, 2976 (1993).
- [24] Y. M. Dai, A. Akrap, J. Schneeloch, R. D. Zhong, T. S. Liu, G. D. Gu, Q. Li, and C. C. Homes, *Phys. Rev. B* **90**, 121114 (2014).
- [25] D. Wu, N. Barišić, P. Kallina, A. Faridian, B. Gorshunov, N. Drichko, L. J. Li, X. Lin, G. H. Cao, Z. A. Xu, N. L. Wang, and M. Dressel, *Phys. Rev. B* **81**, 100512 (2010).
- [26] Y. M. Dai, B. Xu, B. Shen, H. Xiao, H. H. Wen, X. G. Qiu, C. C. Homes, and R. P. S. M. Lobo, *Phys. Rev. Lett.* **111**, 117001 (2013).
- [27] K. Takenaka, R. Shiozaki, S. Okuyama, J. Nohara, A. Osuka, Y. Takayanagi, and S. Sugai, *Phys. Rev. B* **65**, 092405 (2002).
- [28] M. Yi, Z.-K. Liu, Y. Zhang, R. Yu, J.-X. Zhu, J. Lee, R. Moore, F. Schmitt, W. Li, S. Riggs, J.-H. Chu, B. Lv, J. Hu, M. Hashimoto, S.-K. Mo, Z. Hussain, Z. Mao, C. Chu, I. Fisher, Q. Si, Z.-X. Shen, and D. Lu, *Nature Commun.* **6**, 7777 (2015).
- [29] Y. M. Dai, H. Miao, L. Y. Xing, X. C. Wang, P. S. Wang, H. Xiao, T. Qian, P. Richard, X. G. Qiu, W. Yu, C. Q. Jin, Z. Wang, P. D. Johnson, C. C. Homes, and H. Ding, *Phys. Rev. X* **5**, 031035 (2015).
- [30] J. K. Dong, S. Y. Zhou, T. Y. Guan, H. Zhang, Y. F. Dai, X. Qiu, X. F. Wang, Y. He, X. H. Chen, and S. Y. Li, *Phys. Rev. Lett.* **104**, 087005 (2010).
- [31] K. Haule, C.-H. Yee, and K. Kim, *Phys. Rev. B* **81**, 195107 (2010).
- [32] Z. P. Yin, K. Haule, and G. Kotliar, *Nature Phys.* **7**, 294 (2011).
- [33] T. Yoshida, S.-i. Ideta, I. Nishi, A. Fujimori, M. Yi, R. Moore, S.-K. Mo, D. Lu, Z.-X. Shen, Z. Hussain, K. Kihou, C. H. Lee, A. Iyo, H. Eisaki, and H. Harima, *Front. Phys.* **2**, 17 (2014).
- [34] T. Sato, K. Nakayama, Y. Sekiba, P. Richard, Y.-M. Xu, S. Souma, T. Takahashi, G. F. Chen, J. L. Luo, N. L. Wang, and H. Ding, *Phys. Rev. Lett.* **103**, 047002 (2009).
- [35] G. Lee, H. S. Ji, Y. Kim, C. Kim, K. Haule, G. Kotliar, B. Lee, S. Khim, K. H. Kim, K. S. Kim, K.-S. Kim, and J. H. Shim, *Phys. Rev. Lett.* **109**, 177001 (2012).
- [36] Y. Li, Z. Yin, X. Wang, D. W. Tam, D. L. Abernathy, A. Podlesnyak, C. Zhang, M. Wang, L. Xing, C. Jin, K. Haule, G. Kotliar, T. A. Maier, and P. Dai, *Phys. Rev. Lett.* **116**, 247001 (2016).
- [37] D. Fobes, I. A. Zaliznyak, Z. Xu, R. Zhong, G. Gu, J. M. Tranquada, L. Harriger, D. Singh, V. O. Garlea, M. Lumsden, and B. Winn, *Phys. Rev. Lett.* **112**, 187202 (2014).
- [38] M. M. Qazilbash, M. Brehm, B.-G. Chae, P.-C. Ho, G. O. Andreev, B.-J. Kim, S. J. Yun, A. V. Balatsky, M. B. Maple, F. Keilmann, H.-T. Kim, and D. N. Basov, *Science* **318**, 1750 (2007).
- [39] Z. P. Yin, K. Haule, and G. Kotliar, *Phys. Rev. B* **86**, 195141 (2012).
- [40] J. Mravlje, M. Aichhorn, T. Miyake, K. Haule, G. Kotliar, and A. Georges, *Phys. Rev. Lett.* **106**, 096401 (2011).

# Supplementary material for Observation of an Emergent Coherent State in Iron-Based Superconductor $\text{KFe}_2\text{As}_2$

Run Yang,<sup>1,2</sup> Zhiping Yin,<sup>3,\*</sup> Yilin Wang,<sup>2</sup> Yaomin Dai,<sup>2</sup> Hu Miao,<sup>2</sup> Bing Xu,<sup>4</sup> Xianggang Qiu,<sup>1,5,†</sup> and Christopher C. Homes<sup>2,‡</sup>

<sup>1</sup>*Beijing National Laboratory for Condensed Matter Physics, Institute of Physics, Chinese Academy of Sciences, P.O. Box 603, Beijing 100190, China*

<sup>2</sup>*Condensed Matter Physics and Materials Science Division, Brookhaven National Laboratory, Upton, New York 11973, USA*

<sup>3</sup>*Center for Advanced Quantum Studies and Department of Physics, Beijing Normal University, Beijing 100875, China*

<sup>4</sup>*Center for High Pressure Science and Technology Advanced Research, Beijing 100094, China*

<sup>5</sup>*Collaborative Innovation Center of Quantum Matter, Beijing 100084, China*

(Dated: July 14, 2017)

## EXPERIMENTAL DETAILS

High-quality single crystals of  $\text{KFe}_2\text{As}_2$  with good cleavage planes (001) were synthesized using self-flux method [1]. The resistivity measurement of  $\text{KFe}_2\text{As}_2$  was performed using a Quantum Design physical property measurement system (PPMS). The reflectivity from a freshly-cleaved surface has been measured at a near-normal angle of incidence using Fourier transform infrared spectrometers (Bruker Vertex 80v and IFS 113v) for light polarized in the  $ab$ -plane using an *in situ* evaporation technique [2]. Data from  $\sim 15$  to  $45\,000\text{ cm}^{-1}$  were collected at different temperatures from  $\sim 5$  to  $300\text{ K}$  using an ARS Helitran open-flow cryostat. The optical conductivity has been determined from a Kramers-Kronig analysis of the reflectivity  $R(\omega)$ . Because the measurement is performed over a finite energy range, extrapolations are necessary for  $\omega \rightarrow 0, \infty$  [3]. Below the lowest measured frequency, the Hagen-Rubens relation [ $R(\omega) = 1 - A\sqrt{\omega}$ ] for a metal is used, while above the highest-measured frequency ( $45\,000\text{ cm}^{-1}$ ),  $R(\omega)$  is assumed to be constant up to  $7\text{ eV}$ , above which a free-electron response ( $\omega^{-4}$ ) is used [4].

Figure S1 shows the temperature dependence of the reflectivity  $R(T, \omega)$ . In the far-infrared region, it is characterized by typical metallic response, approaching unity at zero frequency. Above  $150\text{ K}$ , the reflectivity displays little temperature dependence; for  $T < 150\text{ K}$ , it increases quickly with decreasing temperature. Below  $50\text{ K}$ , an upturn emerges in  $R(T, \omega)$  below about  $100\text{ cm}^{-1}$ , indicating enhanced metallicity. In the inset of Fig. S1, we use the fits to the real and imaginary parts of the optical conductivity to determine  $\sigma_{\text{DC}} \equiv \sigma_1(\omega \rightarrow 0)$  where  $\rho = 1/\sigma_{\text{DC}}$ ; the result agrees well with the transport measurements, demonstrating the self-consistent nature of the analysis.

## ELECTRONIC STRUCTURE CALCULATIONS

The calculations are performed using an *ab-initio* method for correlated electron materials based on a combination of density functional theory (DFT) and dynamical mean field theory (DMFT) [5, 6]. The DMFT results improve the DFT description of the electronic structure of strongly correlated materials, in particular the iron-based superconductors, predicting the correct magnitude of the ordered magnetic moments [7], and improving the description of the electron spectral functions, Fermi surfaces [5, 6], charge response function such as optical conductivity [6], and spin dynamics [7]. For the sake of consistency, we use in this work the same crystal structure, Hubbard  $U = 5.0\text{ eV}$ , Hund's rule coupling  $J_H = 0.8\text{ eV}$  as in previous work [5, 7].

## DRUDE-LORENTZ FIT

The optical conductivity can be fitted with the Drude-Lorentz model with a complex dielectric function  $\tilde{\epsilon} = \epsilon_1 + i\epsilon_2$ ,

$$\tilde{\epsilon}(\omega) = \epsilon_\infty - \sum_j \frac{\omega_{p,j}^2}{\omega^2 + i\omega/\tau_j} + \sum_k \frac{\Omega_k^2}{\omega_k^2 - \omega^2 - i\omega\gamma_k}, \quad (\text{S1})$$

where  $\epsilon_\infty$  is the real part at high frequency. In the first sum  $\omega_{p,j}^2 = 4\pi n_j e^2/m_j^*$  and  $1/\tau_j$  are the square of the plasma frequency and scattering rate for the delocalized (Drude) carriers in the  $j$ th band, respectively, and  $n_j$  and  $m_j^*$  are the

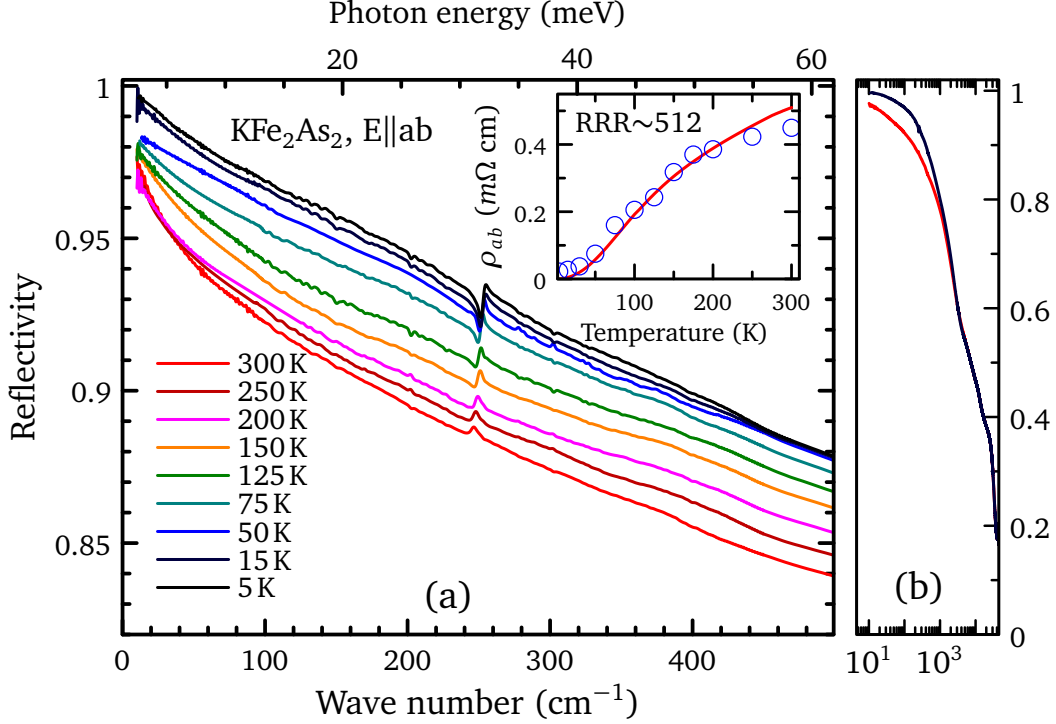


Figure S1. (a) Temperature-dependent reflectivity of KFe<sub>2</sub>As<sub>2</sub> in the far-infrared region for light polarized in the Fe-As planes. Inset: The in-plane resistivity, the residual-resistivity ratio (RRR) is about 512. The circles denote the zero-frequency extrapolation of the optical conductivity,  $\sigma_{DC} \equiv \sigma_1(\omega \rightarrow 0)$ . (b) The reflectivity in the high-frequency range at 300 and  $\sim 5$  K.

carrier concentration and effective mass. In the second summation,  $\omega_k$ ,  $\gamma_k$  and  $\Omega_k$  are the position, width, and strength of the  $k$ th vibration or bound excitation. The complex conductivity is  $\tilde{\sigma}(\omega) = \sigma_1 + i\sigma_2 = -2\pi i\omega[\tilde{\epsilon}(\omega) - \epsilon_\infty]/Z_0$ , where  $Z_0 \simeq 377 \Omega$  is the impedance of free space, yielding units for the conductivity of  $\Omega^{-1}\text{cm}^{-1}$ . The real part of the optical conductivity is then

$$\sigma_1(\omega) = \frac{2\pi}{Z_0} \left[ \sum_j \frac{\omega_{p,j}^2 \tau_j}{(1 + \omega^2 \tau_j^2)} + \sum_k \frac{\gamma_k \omega^2 \Omega_k^2}{(\omega_k^2 - \omega^2)^2 + \gamma_k^2 \omega^2} \right]. \quad (\text{S2})$$

The data have been fit using a non-linear least-squares technique. At high temperature (300 K), the conductivity up to 22000  $\text{cm}^{-1}$  is reproduced quite well with two Drude and two Lorentz components [Fig. S2(a)]. However, below  $T^* \sim 155$  K, another Drude component was added to fit the low-energy optical response, shown in Fig. S2(b) at 5 K. Upon cooling, this newly-formed Drude component is gradually enhanced and dominates the DC conductivity at low temperature; the temperature-dependent fitting parameters are summarized in Table I. We note that this analysis

Table I. Temperature dependence of the plasma frequency  $\omega_{p,j}$ , scattering rate  $1/\tau_j$  of the Drude components, the position  $\omega_k$ , width  $\gamma_i$ , and the oscillator strength  $\Omega_k^2 = S_k \omega_k^2$  for the bound excitations. Unless otherwise indicated, all units are in  $\text{cm}^{-1}$ , where 1 eV=8065.5  $\text{cm}^{-1}$ .

$T$ (K)	Drude						Lorentz								
	$\omega_{p,1}$	$1/\tau_1$	$\omega_{p,2}$	$1/\tau_2$	$\omega_{p,3}$	$1/\tau_3$	$\omega_1$	$\gamma_1$	$S_1$	$\omega_2$	$\gamma_2$	$S_2$	$\omega_3$	$\gamma_3$	$S_3$
300	3482	750	13490	1782			1907	4922	35	10301	27796	31	22244	17632	1.03
200	4169	427	13571	1782			2006	5686	37	10530	28184	30	22282	17013	0.94
150	4438	372	13517	1750	818	24	1925	5405	37	10402	28123	30	22275	17126	0.95
75	4458	219	13517	1753	2342	54	1909	5658	40	10478	28157	30	22254	17168	0.96
50	4436	141	13503	1722	2807	27	1920	5958	44	10656	28324	30	22323	16819	0.91
30	4426	131	13502	1722	2875	8.4	1961	5341	47	10487	28187	30	22249	17061	0.95
5	4346	110	13503	1722	2980	1.2	1979	5968	43	10641	28308	29	22274	17112	0.96

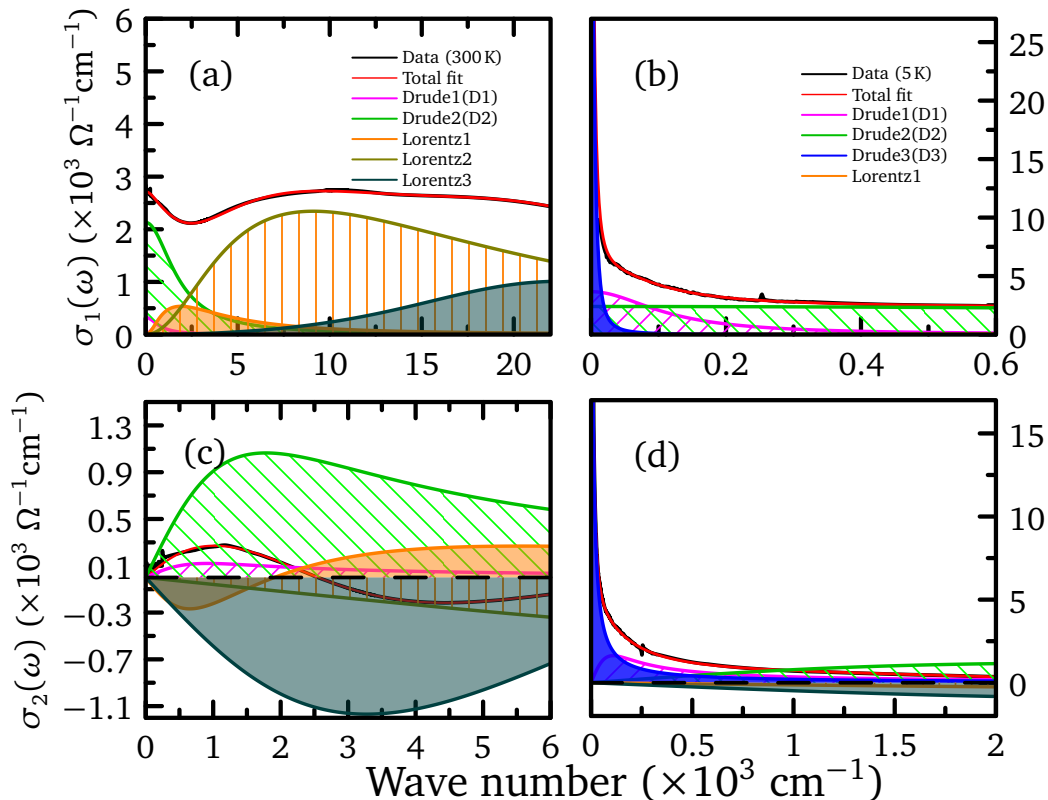


Figure S2. (a) The fit using the two-Drude model to the real part and imaginary parts of the optical conductivity of  $\text{KFe}_2\text{As}_2$  at 300 K up to  $22000 \text{ cm}^{-1}$ . The red line through the data is the fit which is decomposed into a broad Drude (green line), a narrow Drude (pink line), and two Lorentz (orange and olive lines) term. (b) The optical conductivity of  $\text{KFe}_2\text{As}_2$  at 5 K below  $1000 \text{ cm}^{-1}$  is described quite well with three Drude components. The results of the fit for the imaginary part of optical conductivity at (c) 300 K, and (d) 5 K.

was extended to fit both the real and imaginary parts of the optical conductivity simultaneously [Figs. S2(c) at 300 K, and S2(d) at 5 K], reproducing the results of the fit to only the real part, an indication of the positive convergence of these fits.

The low-frequency optical conductivity at 15 K has been fit using a two-Drude model; however, the effects of an additional Drude term (three-Drude model) has also been considered. The results shown in Figs. S3(a) and S3(b). We note that while both of these models can reproduce the data quite well, but if we examine the low-frequency region ( $< 1000 \text{ cm}^{-1}$ ) in detail (insets of Fig. S3), we find that the two-Drude model cannot describe the shoulder like structure around  $\sim 800 \text{ cm}^{-1}$  and the sharp peak below  $100 \text{ cm}^{-1}$ . Moreover, when we apply this fit to the reflectivity, shown in Figs. S3(c) and S3(d), it is clear that the two-Drude model does not reproduce the correct magnitude and curvature of the reflectivity, while the three-Drude model does. This indicates that the introduction of a new, narrow Drude component, resulting in three Drude terms, better describes the nature of  $\text{KFe}_2\text{As}_2$  at low temperature, and that a new coherent state emerges below the incoherent-coherent crossover around 155 K.

### SPECTRAL WEIGHT ANALYSIS

In Fig. S4(a), we plotted the square of plasma frequency of the emergent Drude term ( $\omega_{p,D3}^2$ ), from 150 to 5 K. It increases continuously and follows a mean-field temperature dependence, reflecting the emergent nature of the new coherent Drude peak. In Fig. S4(b), we carried out the spectral weight analysis, where the spectral weight is defined as

$$W(\omega_c) = \int_0^{\omega_c} \sigma_1(\omega) d\omega, \quad (\text{S3})$$

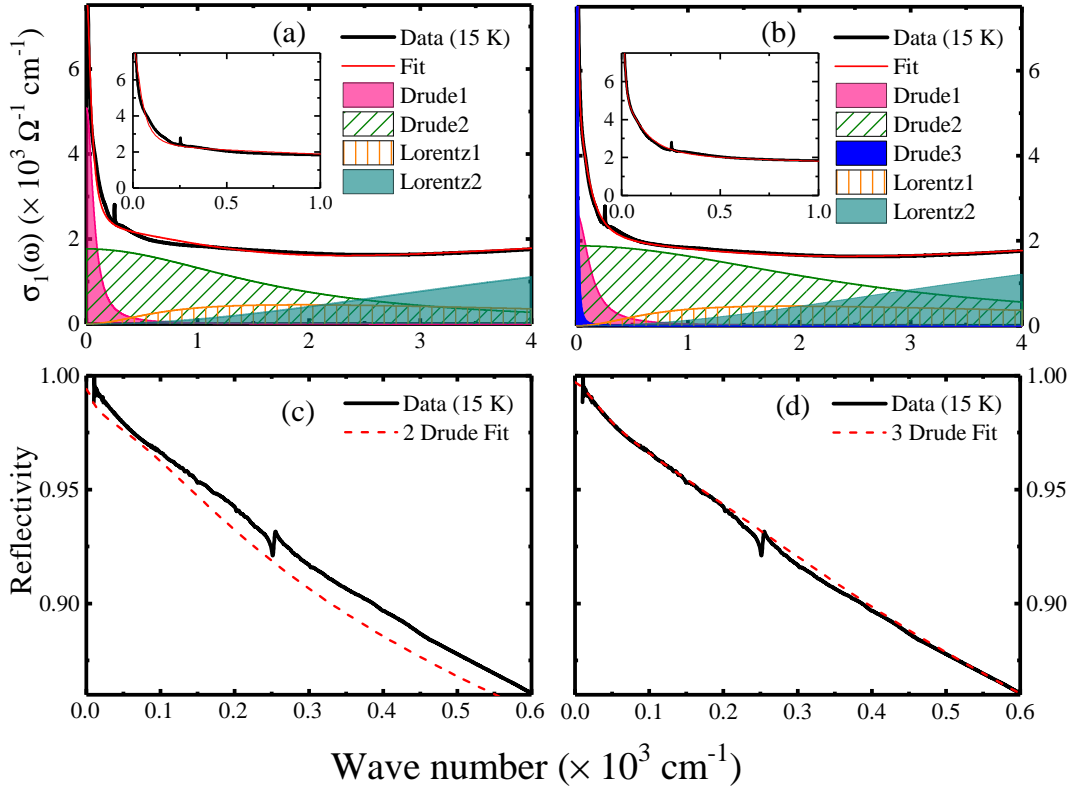


Figure S3. The black solid curve is the measured  $\sigma_1$  of  $\text{KFe}_2\text{As}_2$  at 15 K up to  $6000 \text{ cm}^{-1}$ . The red line through the data is the fit which is decomposed into two Drude, one Lorentz components (a) and three Drude, one Lorentz components. The insets are the zooming in of the data and corresponding fitting below  $1000 \text{ cm}^{-1}$ . In (c) and (d), the black solid curves are the measured reflectivity of  $\text{KFe}_2\text{As}_2$  at 15 K, the red dashed curve is the reflectivity converted from the fitting optical conductivity in (a) and (b).

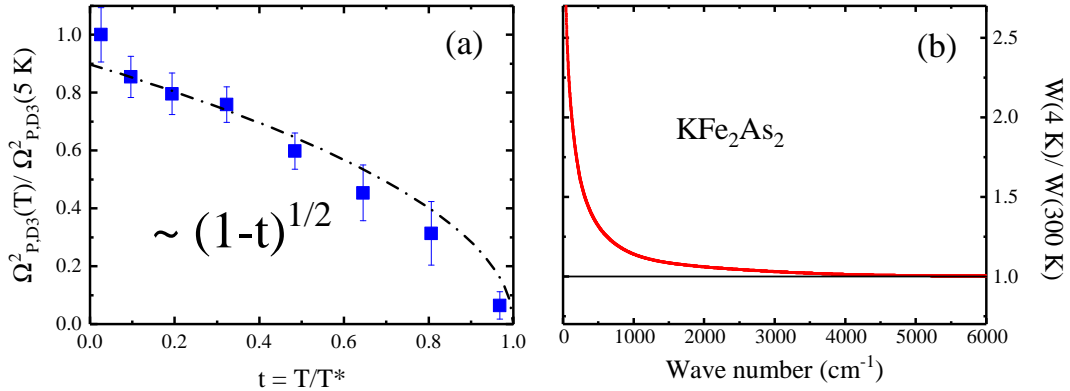


Figure S4. (a) The square of the normalized plasma frequency for the newly formed narrow Drude (D3) versus the reduced temperature; the dash-dot line denotes mean-field behavior (the incoherent-coherent crossover temperature  $T^* \sim 155 \text{ K}$ ). (b) Ratio of the integrated spectral weight  $W(5 \text{ K})/W(300 \text{ K})$ , where as a function of cut-off frequency  $\omega_c$  in  $\text{KFe}_2\text{As}_2$ .

the low-temperature (5 K) spectral weight has been normalized to the room-temperature value. From the result, we notice that the spectral weight in the low-energy region strongly enhanced and gradually recovers above  $5000 \text{ cm}^{-1}$ , indicating spectral weight transfer from high ( $> 0.4 \text{ eV}$ ) to low energy, which is consistent with the fitting results. These results indicate that upon cooling, localized electrons start to form coherent quasiparticles.

Comparing with other iron pnictides such as optimally-doped  $\text{Ba}_{1-x}\text{K}_x\text{Fe}_2\text{As}_2$  [8], below 300 K, in  $\text{KFe}_2\text{As}_2$ , we have not observed the spectral weight transfer from the low- to high-energy area, which has been attributed to the

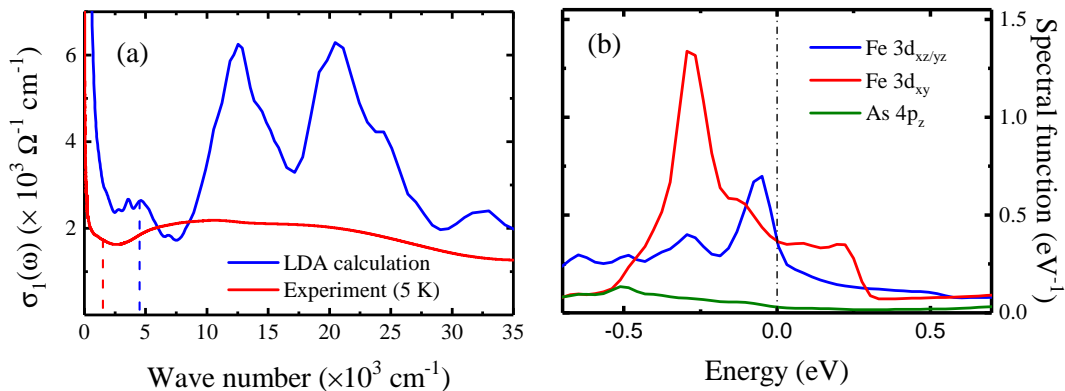


Figure S5. (a) The red curve is the real part of the  $ab$ -plane optical conductivity  $\sigma_1(\omega)$  of  $\text{KFe}_2\text{As}_2$  as a function of frequency at 5 K. The blue curve is the  $\sigma_1(\omega)$  plot calculated within the density function of theory (DFT). The dashed lines represent the cut off frequency selected to estimate the plasma frequency of itinerant carriers. (b) is  $\text{KFe}_2\text{As}_2$ 's density of states, calculated through DFT. The dashed line denotes the Fermi level.

Hund's rule coupling effect. Wang *et al.* proposed that since the high pnictogen height in  $\text{KFe}_2\text{As}_2$  corresponding to strong Hund's coupling, so that the localizing effect is completed above 300 K [8]. The Hund's coupling effect offers us a perfect platform to observe the delocalization in  $\text{KFe}_2\text{As}_2$  below  $T^*$ .

### ELECTRONIC CORRELATIONS

In correlated materials, it has been pointed out that the electronic correlations could modify the kinetic energy of the itinerant carriers and make the  $K_{\text{exp}}/K_{\text{band}}$ , where  $K_{\text{exp}}$  is the experimental kinetic energy,

$$K_{\text{exp}}(\omega_c) = \frac{2\hbar^2 c_0}{\pi e^2} \int_0^{\omega_c} \sigma_1(\omega) d\omega \quad (\text{S4})$$

and  $K_{\text{band}}$  is the kinetic energy estimated by the electronic structure calculation), less than unity [9]. Since the kinetic energy of the itinerant carriers is proportional to the spectral weight of the Drude part of  $\sigma_1(\omega)$ , to estimate the correlation in  $\text{KFe}_2\text{As}_2$ , we've calculated the low-energy spectral weight below the cut off frequency  $\omega_c$ , indicated by the dashed lines in Fig. S5(a) for the experimental and calculated optical conductivity. The  $K_{\text{exp}}/K_{\text{band}}$  value for  $\text{KFe}_2\text{As}_2$  is around 0.2, which is close to the value for optimally-doped  $\text{La}_{1-x}\text{Sr}_x\text{CuO}_4$  [9], indicating a strongly correlated material. In Fig. S5(b), we calculated the density of state with LDA, the result is quite different than that calculated by DMFT [Figs. 4(d) and Fig. 4(e) in the main text], especially in  $d_{xy}$  orbital, suggesting that the incoherent-coherent crossover is the due to correlation effects in Hund's metal.

In addition, we notice that in the LDA-calculated optical conductivity, there are two sharp peaks centered at  $\sim 12500$  and  $20000 \text{ cm}^{-1}$ , while in the experimental data, the two peaks are located at  $10000$  and  $19000 \text{ cm}^{-1}$ . These two peaks most likely arise from optical transitions between Fe  $3d$  bands; electronic correlations could modify the bands and change the transition energy. On the other hand, because of the strong electronic interaction, there are no well-defined quasiparticles at high-energy area, so the system will become dissipative, which could broaden an optical transition.

\* yinzhiping@bnu.edu.cn

† xgqiu@iphy.ac.cn

‡ homes@bnl.gov

- [1] J. S. Kim, E. G. Kim, G. R. Stewart, X. H. Chen, and X. F. Wang, "Specific heat in  $\text{KFe}_2\text{As}_2$  in zero and applied magnetic field," *Phys. Rev. B* **83**, 172502 (2011).
- [2] Christopher C. Homes, M. Reedyk, D. A. Crandles, and T. Timusk, "Technique for measuring the reflectance of irregular, submillimeter-sized samples," *Appl. Opt.* **32**, 2976–2983 (1993).
- [3] M. Dressel and G. Grüner, *Electrodynamics of Solids* (Cambridge University Press, Cambridge, 2001).

- [4] F. Wooten, *Optical Properties of Solids* (Academic Press, New York, 1972) pp. 244–250.
- [5] Z. P. Yin, K. Haule, and G. Kotliar, “Kinetic frustration and the nature of the magnetic and paramagnetic states in iron pnictides and iron chalcogenides,” *Nature Mater.* **10**, 932–935 (2011).
- [6] Kristjan Haule, Chuck-Hou Yee, and Kyoo Kim, “Dynamical mean-field theory within the full-potential methods: Electronic structure of CeIrIn<sub>5</sub>, CeCoIn<sub>5</sub>, and CeRhIn<sub>5</sub>,” *Phys. Rev. B* **81**, 195107 (2010).
- [7] Z. P. Yin, K. Haule, and G. Kotliar, “Magnetism and charge dynamics in iron pnictides,” *Nature Phys.* **7**, 294–297 (2011).
- [8] N L Wang, W Z Hu, Z G Chen, R H Yuan, G Li, G F Chen, and T Xiang, “High energy pseudogap and its evolution with doping in Fe-based superconductors as revealed by optical spectroscopy,” *J. Phys.: Condens. Mat.* **24**, 294202 (2012).
- [9] M. M. Qazilbash, J. J. Hamlin, R. E. Baumbach, Lijun Zhang, D. J. Singh, M. B. Maple, and D. N. Basov, “Electronic correlations in the iron pnictides,” *Nature Phys.* **5**, 647–650 (2009).